Phase behaviour of parallel hard rods in confinement: an Onsager theory study

2010 J. Phys.: Condens. Matter 22 175002

(http://iopscience.iop.org/0953-8984/22/17/175002)

IOP Publishing Journal of Physics: Condensed Matter

J. Phys.: Condens. Matter **22** (2010) 175002 (12pp) doi:10.1088/0953-8984/22/17/175002

Phase behaviour of parallel hard rods in confinement: an Onsager theory study

Alexandr Malijevský[1,2] **and Szabolcs Varga**[3]

[1] Department of Chemical Engineering, Imperial College London, South Kensington Campus, London SW7 2BZ, UK
[2] E Hála Laboratory of Thermodynamics, Institute of Chemical Process Fundamentals of the ASCR, v. v. i., 165 02 Prague 6, Czech Republic
[3] Institute of Physics, University of Pannonia, PO Box 158, Veszprém, H-8201, Hungary

Received 11 January 2010, in final form 26 February 2010
Published 23 March 2010
Online at stacks.iop.org/JPhysCM/22/175002

Abstract
The effect of confinement on the positional ordering is examined in a system of parallel hard cylinders using the second virial theory of Onsager. Hard cylinders are arranged in a slit-like pore (two parallel planar hard walls) in such a way that the long axes of the particles are perpendicular to the surface of confining hard walls. We have incorporated the theories of the bulk and the confined systems into a single formalism, where a w_{ij} kernel function provides the link between the bulk and confined systems. It is shown that the presence of hard walls inhibits the second order nematic–smectic A phase transition irrespective of the value of the wall-to-wall separation. Instead, due to accommodation problems of the cylinders into the pore, an infinite number of first order layering phase transitions appears. Coexisting curves, corresponding to the equilibrium between two phases having n and $n + 1$ smectic-like periods, are bounded with lower critical points. The gap between the average densities of the coexisting phases shrinks with increasing pore width, while the properties of the critical points monotonically move towards those of the nematic–smectic A phase transition of the bulk system ($d \to \infty$). The effect of only one hard wall is related to the bulk nematic–smectic A phase transition since a critical wetting transition of the wall induced layering takes place.

(Some figures in this article are in colour only in the electronic version)

1. Introduction

Bulk and confined systems of mesogenic molecules show very interesting phase behaviour. It is now well understood that the anisotropic hard body interactions can alone give rise to the formation of mesophases such as the nematic, smectic and columnar phases [1, 2]. Extensive simulation studies of the system of hard spherocylinders [3, 4] have shown that the stability of mesophases depends on the shape anisotropy of the molecule. For example, more elongated particle shape is required to stabilize the nematic phase than the smectic one. The presence of a substrate or confining walls may strongly affect the stability and the structure of mesophases due to the interplay between adhesive and cohesive forces. Depending on the wall–particle interaction, the wall can either induce homeotropic or planar anchoring at the wall. The presence of a substrate not only affects the structure of isotropic, nematic and more ordered mesophases, but it also induces surface transitions and consequently leads to a complex phase behaviour including wetting and layering transitions. For instance, the isotropic–nematic transition of an anisotropic fluid can be shifted with respect to the bulk depending on the pore width confining the fluid [5]. This is an analogy to the capillary condensation/evaporation phenomena well known from the theory of simple liquids. To get an insight into these interesting phenomena of liquid crystals, the theoretical and simulation studies of mesogenic hard body fluids in a confining slit-like pore can provide very useful information. To understand the physics of confined liquid crystals is of fundamental interest but it plays also an important role in technology, mainly for the application of the material in liquid crystal displays.

Molecular studies of anisotropic fluids in the presence of a solid substrate are devoted mainly to the isotropic and nematic phases where the presence of a single planar hard wall and two parallel hard walls are considered [6–10]. The first comprehensive theoretical study of confined hard rods is due to van Roij *et al* [6]. Restricting the orientations of

the particles into three orthogonal directions the existence of three phenomena are proved: (1) an uniaxial–biaxial nematic surface phase transition, (2) a wetting transition by a nematic film at the wall–isotropic fluid interface and (3) an isotropic–nematic capillary phase transition. In a subsequent study, the MC simulation of freely rotating hard spherocylinders [7] confirms the above findings and shows that the capillary isotropic–nematic transition terminates at a wall separation which is about twice the length of the rod. More recent theoretical studies go beyond the Zwanzig approximation and deal with freely rotating hard anisotropic bodies such as the hard Gaussian [8] and thin plates [9, 10]. In the very recent study of de las Heras *et al* [11] more complicated surface phase phenomena are observed in the system of freely rotating hard spherocylinders due to the presence of conflicting walls.

Much less attention has been paid to the smectic phase, which can be considered as a repetition of 2D nematic layers, and to the nematic–smectic A (N–S) phase transition in the presence of an external field. This may be due to the fact that the smectic phase occurs in very dense systems, where it is difficult to perform both simulation and theoretical studies. The proper sampling of the phase space is a problem in simulation studies, while one has to use a very fine grid size for the accurate representation of the position and orientation dependent one-body density distribution in theoretical methods. We are aware of the DFT studies of de las Heras *et al* [12–14] for the confined smectic phase, where a trial function method is used for the proper representation of the density distribution. They observed both capillary nematization and smectization and layering transitions between two smectic-like phases having n and $n+1$ periods, respectively. Simulation studies of plate-like and rod-like particles focused mainly on the determination of the capillary nematization line [7, 10]. Steuer *et al* [15] examined the stability of isotropic, nematic and smectic ordering in the presence of confinement, using MC simulations. They observed strong stabilization of positional order with respect to isotropic and nematic phases, both in the case of homeotropic and planar anchoring mechanisms. The only weakness of [15] is that the effect of varying pore width was not considered.

In our present study we contribute to the topic of confined nematic and smectic phases by studying the fluid of parallel hard cylinders in the presence of a single wall and narrow slit-like pore confinements. The drawback of the parallel approximation is that we neglect the effect of orientational entropy on the ordering behaviour, i.e. the capillary isotropic–nematic phase transition cannot be studied. However, we can examine the nematic and smectic phases with significantly less computational effort. The concept of studying the nematic and smectic phases of hard body systems in the perfect alignment limit goes back to Hosino *et al* [16]. Using Onsager's second virial theory and a square-wave trial function for the density distribution they point out that the system of parallel hard rods undergoes a N–S phase transition. The exact analysis of the N–S transition of parallel rods is due to Mulder [17]. The main result of [17] is that Onsager theory predicts a second order N–S phase transition at a packing fraction $\eta \approx 0.575$ and the smectic period of the N–S boundary is about 1.4 times the length of the rod. The MC simulation study of Veerman and Frenkel [18] located the transition point at about $\eta \approx 0.44$, which means that the Onsager theory overestimates the stability of the nematic phase. It is worth mentioning that the recently developed fundamental measure theory (FMT) of parallel hard cylinders [19] gives a very reliable equation of state both in the nematic and smectic phases, but it underestimates the N–S transition density. Since the Onsager theory of parallel rods is simple and has proved to be very successful for many systems, such as the mono- and polydisperse liquid crystals [20, 21], and in addition the agreement between FMT and Onsager theory is quite good, we apply the latter for the system of hard cylinders confined between two parallel hard walls. We assume homeotropic alignment for the rods' orientations at the walls, which can be achieved in practice by either a very strong external field or by a very low homeotropic anchoring energy. Apart from the fundamental importance, understanding the structure and phase behaviour of a confined anisotropic fluid is also a prerequisite for the targeted applications in the liquid crystal display industry. A very detailed discussion of both conventional and new alignment techniques at the substrates, such as the submicrometre grooving and photo-alignment, as well as the relevance of various alignment methods used in the liquid crystal display technology are given in the recent review of Ishihara [22].

The main goal of our work is to examine the phase behaviour in the following cases: (i) bulk system, i.e. the system is in the absence of any external field, (ii) semi-infinite system, considering a system with a plane hard wall, and (iii) confined system, where the system is squeezed by two parallel hard walls. In section 2 we re-examine the Onsager theory and we formulate the corresponding density functional in a compact way applicable for both bulk and inhomogeneous systems. In section 3 we discuss our results with the accent on the following problems: does the N–S phase transition detected in bulk persist for the cases of (ii) and (iii)? If so, what is the order of the phase transitions? Do any new phenomena occur if one or two walls are present? What is the phase diagram of the confined system where two free parameters (pore width and the chemical potential) exist? Finally, in section 4 we give some concluding remarks.

2. Onsager theory of aligned hard rods in the bulk phase and in the presence of confinement

We examine very dense systems of hard cylinders, where the particles' long axes can in a good approximation be considered to be parallel so that all their orientational degrees of freedom are suppressed. First the nematic and smectic bulk properties of the orientationally frozen system of hard cylinders are revisited and secondly the effects of a single flat wall and two parallel flat walls are studied. We assume that the long axis of the hard cylinder is perpendicular to the surface of the hard walls, which means that the case of homeotropic anchoring is examined.

Our starting thermodynamic function for both bulk and confined systems is the grand potential functional:

$$\beta\Omega[\rho(\vec{r})] = \beta F[\rho(\vec{r})] + \int \mathrm{d}\vec{r}\,\rho(\vec{r})\{\phi(\vec{r}) - \beta\mu\}, \qquad (1)$$

where β is the inverse temperature, F is the intrinsic free energy functional, μ is the chemical potential, $\phi(\vec{r})$ is the external potential and $\rho(\vec{r})$ is the local number density. The ideal contribution to the free energy functional is given exactly by

$$\beta F_{\mathrm{id}}[\rho(\vec{r})] = \int \mathrm{d}\vec{r}\,\rho(\vec{r})\{\ln(\rho(\vec{r})) - 1\}, \qquad (2)$$

where the de Broglie term is not included, because it does not have effect on the phase behaviour of the system. The excess free energy functional is approximated by the second viral contribution of the virial series

$$\beta F_{\mathrm{ex}}[\rho(\vec{r})] = -\tfrac{1}{2}\int \mathrm{d}\vec{r}_1\,\rho(\vec{r}_1)\int \mathrm{d}\vec{r}_2\,\rho(\vec{r}_2)\,f_{\mathrm{M}}(\vec{r}_{12}), \qquad (3)$$

where the Mayer function, f_{M}, of the hard cylinders with diameter D and length L can be written as a product of two Heaviside functions as follows:

$$f_{\mathrm{M}}(\vec{r}) = -\theta(D - r_\perp)\theta(L - |z|). \qquad (4)$$

In equation (3) it is assumed that the cylinder's long axis is parallel to the z-axis of the chosen coordinate frame and $r_\perp = |\vec{r}_\perp|$ denotes the distance between two particles in the x–y plane. Since we are dealing with the perfectly ordered nematic and the layered (smectic) phases along the z-axis, the local density depends only on the z-coordinate, i.e. $\rho(\vec{r}) = \rho(z)$. For this reason the integrations of the grand potential with respect to $\vec{r}_\perp$ can be performed analytically. In the bulk nematic phase the local density is just a constant, while the bulk smectic phase has a periodic structure along the z-axis. Taking d to be the smectic period (layer spacing), the local number density has to satisfy the periodic condition $\rho(z) = \rho(z + d)$. For this reason it is sufficient to determine the structure of the smectic phase for only one period (e.g. $0 < z < d$). The slit pore breaks the symmetry of the nematic and smectic phases and gives rise to a non-uniform layered structure. To make a formal connection between the grand potential of the confined system and that of the bulk system we define an external potential acting on the centre of the hard cylinder as follows:

$$\phi(z) = \begin{cases} \infty, & z < 0 \\ 0, & 0 < z < d \\ \infty, & z > d, \end{cases} \qquad (5)$$

where d now means the wall-to-wall separation. In order to avoid confusion we mention here that in the case of the bulk calculation the wall–particle potential is zero everywhere and d denotes the smectic period. We use the above wall–particle definition in the sense that the walls are located at $z = 0$ and $z = d$, respectively, and the particles interact with the walls such that the particles' centres feel infinite repulsive potentials at the positions of the walls. Note that we can use the same wall–particle external potential even if hard body interactions take place between the walls and the hard cylinders. Only the positions of the walls should be placed to $z = -L/2$ and $z = d + L/2$, respectively. We will see later that our definition of the external potential and the two meanings of the d variable permit a unified density functional formalism for bulk and confined systems. Taking into account that the density is only nonzero for $0 < z < d$ in the confined system and that the bulk density is periodic in d, the ideal part of the free energy functional can be written as a one-dimensional integral:

$$\frac{\beta F_{\mathrm{id}}}{V}[\rho(z)] = \frac{1}{d}\int_0^d \mathrm{d}z\,\rho(z)\{\ln(\rho(z)) - 1\}. \qquad (6)$$

Combining equations (4) and (3), the excess free energy density functional of both bulk and confined systems can be expressed as

$$\frac{\beta F_{\mathrm{res}}}{V}[\rho(z)] = \frac{D^2\pi}{2d}\int_0^d \mathrm{d}z_1\,\rho(z_1)\int_{z_1-a(z_1)}^{z_1+b(z_1)} \mathrm{d}z_2\,\rho(z_2), \qquad (7)$$

where $a(z) = L$ and $b(z) = L$ in the bulk system, while

$$a(z) = \begin{cases} z, & 0 < z < L \\ L, & z > L \end{cases} \quad \text{and}$$

$$b(z) = \begin{cases} L, & 0 < z < d - L \\ d - z, & d - L < z < d \end{cases}$$

in the slit pore. In the derivation of equation (7) we have used that $\rho(z) = 0$ for $z < 0$ and $z > d$ in the slit pore, and $\rho(z) = \rho(z + d)$ in the bulk smectic A phase. Based on equations (6) and (7) the final form of the grand potential density, $\omega = \frac{\beta\Omega}{V}$, is

$$\omega[\rho(z)] = \frac{1}{d}\int_0^d \mathrm{d}z\,\rho(z)\{\ln(\rho(z)) - 1\} + \frac{D^2\pi}{2d}\int_0^d \mathrm{d}z_1\,\rho(z_1) \times \int_{z_1-a(z_1)}^{z_1+b(z_1)} \mathrm{d}z_2\,\rho(z_2) - \beta\mu\frac{1}{d}\int_0^d \mathrm{d}z\,\rho(z). \qquad (8)$$

The equilibrium structure of the system is determined by that density profile, which minimizes the grand potential functional of the system, i.e. $\frac{\delta\omega}{\delta\rho(z)} = 0$. The resulting Euler–Lagrange equation for confined and bulk systems is

$$\rho(z) = \exp[\beta\mu]\exp\left[-D^2\pi\int_{z-a(z)}^{z+b(z)} \mathrm{d}z_1\,\rho(z_1)\right]. \qquad (9)$$

This equation is self-consistent for the equilibrium density distribution and can be solved by using standard iteration methods. In this work we solve the above equations and evaluate the grand potential by two methods. In the first method we perform all integrations numerically and use Picard's iteration method, while in the second one the Fourier parameterization is applied for the local density distribution. The latter method is very efficient and reliable in the determination of the smectic A structure in bulk systems [21], but it is not tested for confined systems. Therefore, we use the following Fourier ansatz for the density profile both in bulk and confined studies:

$$\rho(z) = \sum_{i=0}^{n} \rho_i \cos(iqz), \qquad (10)$$

where ρ_i is the ith order Fourier coefficient and $q = \frac{2\pi}{d}$ is the wavenumber. Note that zeroth order Fourier coefficient is just the averaged number density ($\rho_0 = \frac{1}{d}\int_0^d \mathrm{d}z\, \rho(z)$). After substitution of equation (10) into (9) and using the orthogonality properties of the cosine functions ($\int_0^d \mathrm{d}z\, \cos(iqz)\cos(jqz) = \frac{d}{2}(\delta_{ij} + \delta_{j0}\delta_{i0})$) it can be shown that the Fourier coefficients obey the following set of coupled nonlinear equations:

$$\rho_i = (1+\delta_{i,0})\frac{\exp[\beta\mu]}{2d}\int_0^d \mathrm{d}z\, \cos(iqz) \times \exp\left[-D^2\pi\int_{z-a(z)}^{z+b(z)} \mathrm{d}z_1 \rho(z_1)\right] \qquad (i = 0,\ldots,n). \tag{11}$$

The solution of the above set of equations at a given chemical potential provides the equilibrium Fourier coefficients and density profile of the system. In the case of the bulk smectic phase one further step is required which determines the equilibrium smectic period (discussed later). The advantage of the Fourier expansion over the iterative method is that the number of unknown Fourier coefficients ($n+1$) can be substantially lower than the number of discrete density points of the iterative method in the numerical implementation. In addition, the integrals of the cosine function can be performed analytically. The solution of equation (11) at a given chemical potential shows that ρ_i decays rapidly with increasing i. For example in the bulk calculations it has been more than sufficient to cut the series at the 10th shell, i.e. $n = 10$, which guarantees that $|\rho_n| < \varepsilon$, with $\varepsilon = 10^{-4}$. Regarding the confined case, the requested number of Fourier coefficients to get a reliable density profile and grand potential depends strongly on the pore width and the chemical potential. In practice, n increases with the pore width and the chemical potential. We have determined the value of n by the condition $|\rho_n| < \varepsilon$. In addition we have made some checks on the Fourier method by comparing the numerical solution of equation (9) with that given by equation (11). For very wide pores and high chemical potentials we need about 70 Fourier coefficients to reproduce the numerical density profile accurately. In the case of the iterative solution the number of discrete points of the local density and the number of corresponding equations for the density profile depends linearly on the pore width. For example in the wide pore of $d/L = 100$ with grid size of $\Delta z = 0.01L$, equation (9) results in 10 001 coupled equations for the local density. This means that the number of equations can be significantly reduced by using the Fourier method.

In the framework of the Fourier method, the grand potential, which is the minimum of the grand potential functional, can be expressed as a function of ρ_i ($i = 0,\ldots,n$) by substituting equation (10) into (8)

$$\omega = \frac{1}{2\pi}\sum_{i=0}^{n}\rho_i\int_0^{2\pi}\mathrm{d}\varphi\, \cos(i\varphi)\left\{\ln\left(\sum_{j=0}^{n}\rho_j\cos(j\varphi)\right) - 1\right\} + \frac{D^2\pi}{2}\sum_{i,j=0}^{n}\rho_i\rho_j w_{ij} - \beta\mu\rho_0, \tag{12}$$

where $\varphi = \frac{2\pi}{d}z$.

The difference between the bulk and the confined system comes from the w_{ij} function. For bulk system only the diagonal elements of w_{ij} are nonzero

$$w_{ij} = \frac{\sin(iqL)}{iqL}(\delta_{ij} + \delta_{i0}\delta_{j0}), \tag{13a}$$

while for the slit pore w_{ij} reads

$$w_{ij} = \begin{cases} \dfrac{2d-L}{d}, & \text{for } i = j = 0 \\ \dfrac{4}{q^2Ld}\dfrac{\cos^2(jqL/2) - \cos^2(iqL/2)}{j^2 - i^2}, & \text{for } i \neq j \\ \dfrac{\sin(iqL)}{iqL}\dfrac{d-L}{d}, & \text{for } i = j \neq 0. \end{cases} \tag{13b}$$

Note that if we consider q and d as independent variables, which is not the case here, equations (13a) and (13b) would be identical in the limit of $d \to \infty$. We can see from equations (12) and (13) that only the calculation of the ideal free energy term requires a single numerical integration in Fourier method, while even double integrals have to be performed numerically in the iterative procedure to obtain the grand potential (see equation (8)). From the numerical point of view there is one important difference between the bulk and the confined systems. In the slit pore the wall-to-wall separation is fixed in advance, while the smectic period of the bulk system is that which minimizes the grand potential. So the variable d in the Euler–Lagrange equation, equation (9), is a fixed parameter for the confined system but a free parameter for the bulk smectic phase. In order to get the grand potential of the bulk smectic system for a given chemical potential using the iterative procedure, the density profile and the grand potential are determined as functions of the smectic period from equations (8) and (9). Then, the minimum of the grand potential gives the equilibrium grand potential, the smectic period and the corresponding density profile. This procedure is easier in the Fourier method, because the minimum condition of the grand potential with respect to the smectic period is directly obtained from $\frac{\delta\omega}{\delta q} = 0$. Using equation (12) we get a simpler equation for the equilibrium wavenumber in the Fourier method:

$$\sum_{i,j=0}^{n}\rho_i\rho_j\frac{\partial w_{ij}}{\partial q} = 0. \tag{14}$$

Numerical solution of equations (11) and (14) provides $n+1$ equilibrium Fourier coefficients and the wavenumber at a given chemical potential. After this, we can compute the equilibrium grand potential of the system from equation (12). In summary, the number of unknowns is $n+1$ for the confined study, while it is $n+2$ for the bulk study in the Fourier method. We can see that it is straightforward to implement the Fourier method for both confined and the bulk system. However the efficiency of the Fourier method depends on the suitability of the ansatz given by equation (10), which is clearly approved for the truly periodic smectic phase but might be more delicate in cases where the density profiles exhibit damped oscillatory

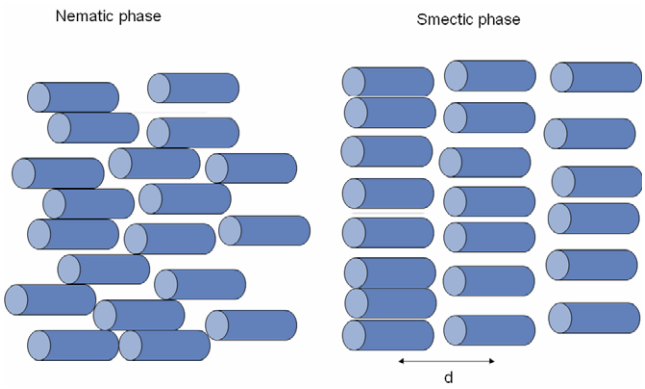

Figure 1. Sketch of the nematic phase (left side) and the smectic A phase (right side) of the system of parallel hard cylinders.

behaviour with rapidly changing amplitudes and where the structure is not exactly periodic. Moreover, a set of $n + 1$ or $n + 2$ plausible initial values has to be set before the calculations. In contrast, e.g. Picard's iteration method is very robust and gives a solution practically regardless of the initial density profile and it can be used for both confined and semi-infinite systems. The drawback of the iterative method is the inefficiency for bulk phase calculations.

At the end of this section we explain how to determine the phase boundaries. Let us assume that two phases (structures), α_1 and α_2, are in coexistence at a given chemical potential. This implies that there are two different solutions of equation (9) (equation (11)) using the iterative method (Fourier method). These structures are in coexistence if the grand potentials of the phases α_1 and α_2 are equal, i.e. $\omega(\alpha_1) = \omega(\alpha_2)$. In the bulk system such a condition corresponds to equality of pressures. In confined systems the same condition has to be applied in order to guarantee the minimum condition of the grand potential for any pore width. We use the $\omega(\alpha_1) = \omega(\alpha_2)$ condition for the location of the layering transition pore width at which the two layered structures have the same grand potential.

3. Results and discussion

Prior to study of the structure and phase behaviour of perfectly aligned hard cylinders in a slit pore we revisit the bulk behaviour of the model. In the bulk phase the system exhibits nematic, smectic A and solid phases (see figure 1). The solid phase is not considered in our study. Fourier expansion results of the Onsager theory for the nematic–smectic A (N–S) phase transition are presented in figure 2. We only show the first and second derivative of the grand potential, which are determined according to the procedure in the appendix. The presence of a kink in the first derivative of the grand potential with respect to the chemical potential suggests that the transition is of the second order (figure 2(a)). Examining the second derivative of the grand potential with respect to the chemical potential, we can see that a clear discontinuity is present (figure 2(b)). Therefore the N–S transition of hard cylinders is of second order on the level of Onsager theory. Since the first derivative

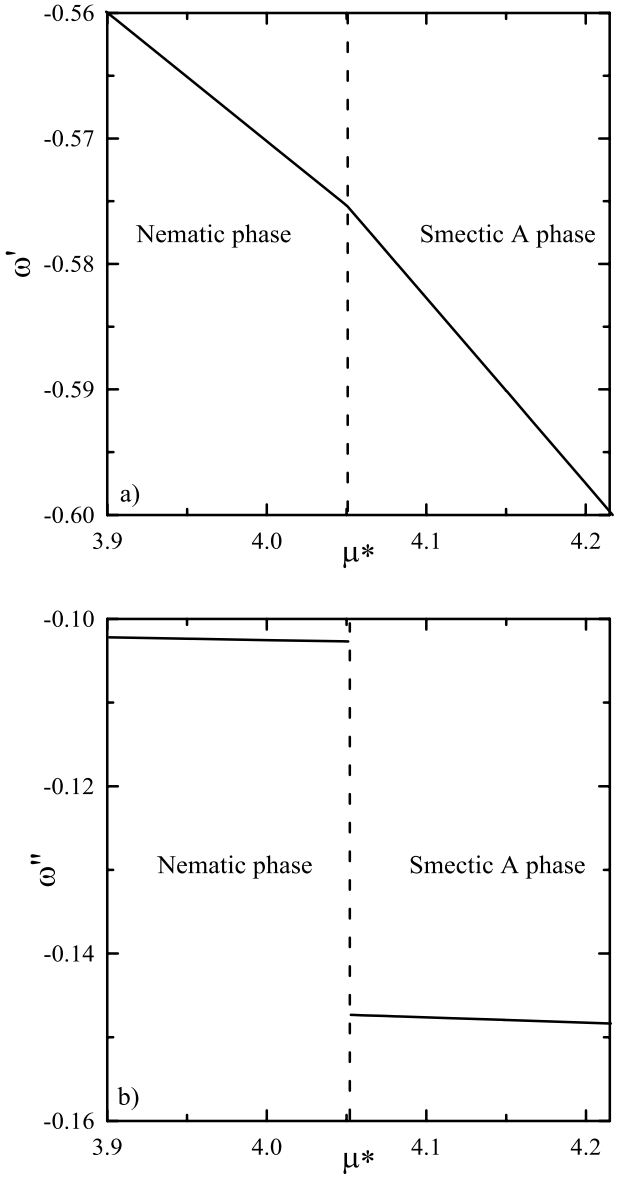

Figure 2. Chemical potential dependence of the derivatives of the grand potential in the region of the nematic–smectic A phase transition of the bulk hard cylinder system. The first and second derivatives of the grand potential density are shown in (a) and (b), respectively. The plotted quantities are defined as $\omega' = \frac{\mathrm{d}\omega^*}{\mathrm{d}\mu^*}$ and $\omega'' = \frac{\mathrm{d}^2\omega^*}{\mathrm{d}\mu^{*2}}$ where $\omega^* = \beta\Omega v_0/V$ is the dimensionless grand potential density, while $\mu^* = \beta\mu + \ln v_0$ is the dimensionless chemical potential. The volume of a cylinder is $v_0 = D^2\pi L/4$. The vertical dashed line shows the location of the nematic–smectic A phase transition.

of the grand potential is proportional to the mean density (see equation (A.2)), we can easily read the critical value of the packing fraction and that of the chemical potential from the position of the kink in figure 2. The following results are obtained for the packing fraction ($\eta_{\mathrm{N-S}}$), the chemical potential ($\mu_{\mathrm{N-S}}$) and the smectic period ($d_{\mathrm{N-S}}$) of the N–S phase transition: $\eta_{\mathrm{N-S}} = \rho_{\mathrm{N-S}} v_0 \approx 0.5754$, $\mu^*_{\mathrm{N-S}} = \beta\mu_{\mathrm{N-S}} + \ln v_0 \approx 4.0507$ and $d^*_{\mathrm{N-S}} = d_{\mathrm{N-S}}/L \approx 1.3983$, where $v_0 = \frac{\pi}{4} L D^2$ is the volume of the cylinder. Note that

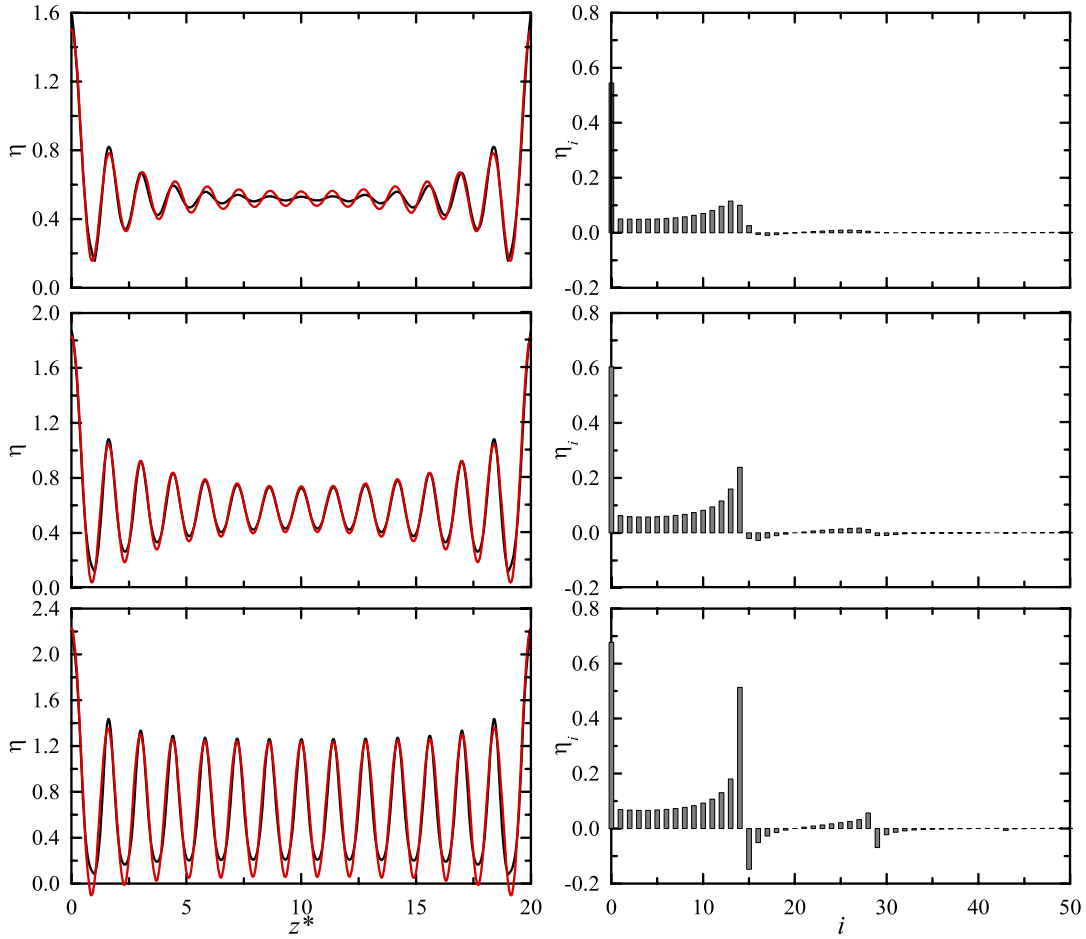

Figure 3. Density profiles and Fourier spectra of hard cylinders between two parallel hard walls. Comparison of Picard's iteration and Fourier expansion methods for three different structures: a strongly damped structure at $\mu^* = 3.5$ (upper left panel), a weakly damped structure at $\mu^* = 4$ (middle left panel) and a smectic-like structure at $\mu^* = 4.5$ (lower left panel). Black curves are the iteration, while the red curves are Fourier expansion results. The Fourier expansion is truncated at $n = 14$ for $\mu^* = 3.5$, while it is done with $n = 20$ for $\mu^* = 4$ and 4.5. Right panels show the Fourier spectrum of the corresponding structures. The Fourier coefficients are dimensionless: $\eta_i = \rho_i v_0$.

these results can be extracted from bifurcation analysis, as well [17]. MC and other theoretical studies also confirm the second order nature of the N–S phase transition [18–20]. Based on a comparison with [17–20] we can say that even though the Onsager theory is very approximate, it is a reasonable theory for the system of parallel hard rods. In the case of freely rotating hard rods the interplay between the orientational and packing entropies gives rise to a weak first order N–S phase transition [4], which slightly changes the scenario.

Now we continue with the fluid confined by two parallel hard walls and we address the issue of what is the effect of the confinement on the phase behaviour of the parallel hard cylinders. In the first step it is worth examining the density profiles for some special chemical potentials at a given pore width using both iterative and Fourier methods. Figure 3 shows three different density profiles in the pore of $d/L = 20$; the first one is taken at a chemical potential corresponding to the nematic phase in bulk, the second one is close to the bulk N–S phase transition, while the third one corresponds to the bulk smectic phase. To see the difference between the iterative and Fourier methods, the accurate iterative and the inadequate Fourier representation results are shown together. At the nematic chemical potential ($\mu^* = 3.5$) one can see that the wall–particle interaction induces an inhomogeneous density profile close to the walls and the nematic structure (no positional order) only survives in the middle of the pore. At the walls, the adsorption of the particles is very strong and a damped layered structure is developed. At $\mu^* = 4$ the bulk phase is still nematic, while the confined system shows a very ordered layered structure. No sign of the homogeneous structure can be seen even in the middle of the pore, instead a weak damped oscillation propagates into the centre of the pore. This means that the walls favour the layered formation against the nematic phase as a consequence of packing effects in the vicinity of the walls. It suggests the hypothesis that the smectic phase can be stabilized by the presence of walls. Finally, at the highest chemical potential, $\mu^* = 4.5$, the density profile of the confined system looks like the structure of a real smectic A phase. We can also see from figure 3 that the iterative and the Fourier methods agree very well. The differences are due to the fact that the Fourier results are determined with unreliable truncation of the Fourier series (equation (10)). The effect of inadequate truncation is the overestimation of the oscillatory behaviour of the local density.

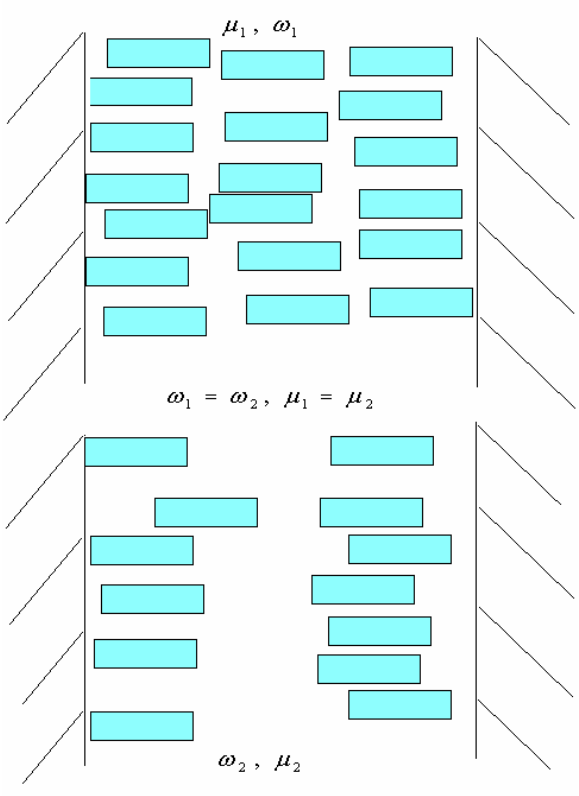

Figure 4. Visual illustration of two coexisting phases exhibiting three (upper panel) and two (lower panel) layers of the fluid in confinement. The systems have identical chemical potentials and wall-to-wall separation.

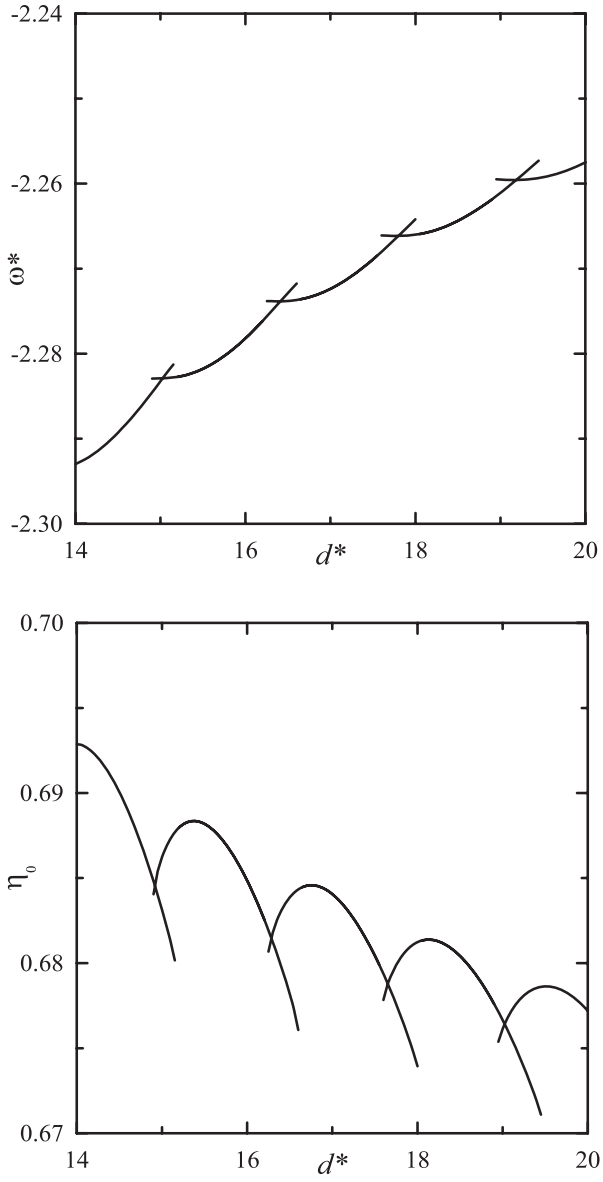

Figure 5. Grand potential density (ω^*) and average number density (η_0) as a function of wall-to-wall distance (d^*) for $\mu^* = 4.5$. The curves are obtained by increasing and decreasing the pore width. In some narrow ranges of the pore width the expansion and compression procedure produces different density profiles. The intersection points of the expansion and compression branches of the grand potential determines the coexistence between two configurations with i and $i + 1$ completed layers.

It may produce even unphysical (negative) values for the density, as seen at the highest chemical potential. The right panel of figure 3 highlights the chemical potential dependence of the Fourier coefficients. Interestingly, the spectrum does not show monotonically decaying behaviour, it oscillates between positive and negative values and dies out slowly. It shows that even 20 terms can be sufficient to get the proper density distribution for $\mu^* = 3.5$, while 35 terms are needed for $\mu^* = 4.5$. In general, the number of coefficients needed in the Fourier method increases both with pore width and chemical potential. Hence, a thorough analysis of the truncation of the series is always essential to find the optimum number of Fourier coefficients in the calculations. Since the two methods produce the same results, from now on we only mention the used method if it is relevant.

The grand potential exhibits very peculiar behaviour with varying pore width. At the chemical potentials of the bulk nematic phase the grand potential is a uniquely invertible function of the pore width and shows oscillatory behaviour. However, it becomes discontinuous, and two solutions of equation (9) can coexist in the smectic regime of the chemical potential. One solution corresponds to a structure with i layers, while the other one has $i + 1$ layers (figure 4 shows a visualization of such a situation). To find both solutions equation (9) is solved upon expansion and compression of the pore, taking advantage of the previously obtained density profile for the next pore width as a starting configuration. In this way we obtain the expansion and compression curves of the grand potential. Figure 5 presents our results for the grand potential and the average packing fraction. We can see that in some intervals of the pore width two branches exist. The branch with the lower (higher) grand potential represents a stable (metastable) phase. The intersection of the two branches in the ω–d plane represents phase coexistence between two smectic-like configurations with i and $i + 1$ periods. The reason why there are two branches is due to the competition of two characteristic length scales. One is the period of the smectic-like structure, while the other is the pore width. An accommodation problem arises when the ratio

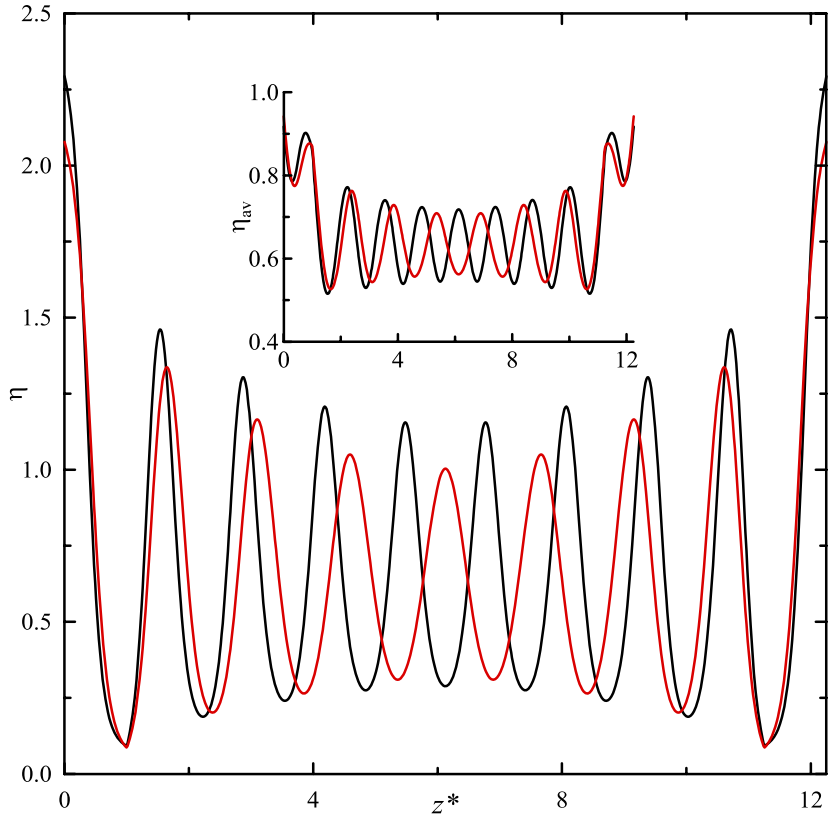

Figure 6. Density profiles of the coexisting S_8 and S_9 phases for $\mu^* = 4.5$. The inset shows the average local packing fractions of the coexisting phases, which is defined as $\eta_{\rm av}(z) = \frac{v_0}{a(z)+b(z)} \int_{z-a(z)}^{z+b(z)} {\rm d}z\, \rho(z)$.

of the pore width and the smectic period is half way between two successive integer numbers, i.e. it is not possible to pack integer numbers of layers between the two walls. Therefore there are regions of the pore width where neither i nor $i+1$ layers can be packed efficiently into the pore. The result of the commensuration effect is a phase transition taking place between two layered structures. Figure 6 presents such a case. One profile consists of 9 layers, which corresponds to 8 smectic periods, while the other has 10 layers (9 smectic periods). We identify the density profiles with the number of periods and use S notation for layered structures. Therefore, S_8–S_9 phase coexistence can be seen in figure 6. Both S_8 and S_9 density profiles are very ordered in the vicinity of the walls, i.e. the adsorption effect of the walls is very strong. To see clearly the packing of the rods, we define an average local packing fraction through averaging the local density only in the interaction region of the pair potential as follows:

$$\eta_{\rm av}(z) = \frac{v_0}{a(z)+b(z)} \int_{z-a(z)}^{z+b(z)} {\rm d}z\, \rho(z). \qquad (15)$$

It is easy to prove that $\eta_{\rm av}(z)$ corresponds to the packing fraction in the homogeneous limit. The inset of figure 6 shows that the average local packing is very high and close to the close packing limit at the walls. We can also see that $\eta_{\rm av}(z)$ has no maximum at the density peaks but in the interstitial regions. This special property of $\eta_{\rm av}(z)$ reflects that the particles staying between two layers interact with the particles of both layers, i.e. the particles of the interstitial regions stay in a very dense environment. Due to the very high value of $\eta_{\rm av}(z)$ at the wall, the possibility of forming solid layers is quite high at $\mu^* = 4.5$, as shown by Steuer *et al* [15]. From the location of the intersection points in the $\omega - d$ plane, we can construct the phase diagram of the confined hard cylinders (see figure 7). Only layering transitions are observed and no N–S phase transition takes place (see the discussion further on). The coexistence curve between the S_i and S_{i+1} structure is almost vertical, and bounded by a lower critical point. The appearance of a lower critical point can be attributed to increasing permeability between the layers and adding/removing a layer has a lower energy cost with decreasing chemical potential. Very narrow pores suppress any phase transitions due to steric effects. For example the minimal value of chemical potential at which the layering transition takes place between S_1 and S_2 structures is observed at $\mu^* = 5.556$ with pore width $d^* = 2.5$. This value of μ^* is well above the N–S critical chemical potential of the bulk phase. We can also see that the critical chemical potential (mean density) goes towards the bulk $\mu_{\rm N-S}(\rho_{\rm N-S})$ with increasing pore width. At the limiting case of infinite wall separation, an infinite number of layers exists, which is equivalent to a stabilization of the smectic A phase. This can be also seen from the behaviour of the coexisting mean densities with increasing wall separation in figure 7(b). At this point it is worth mentioning that the inclusion of the effect of orientational entropy does not change the scenario in the smectic region of the chemical potential, as the confined freely

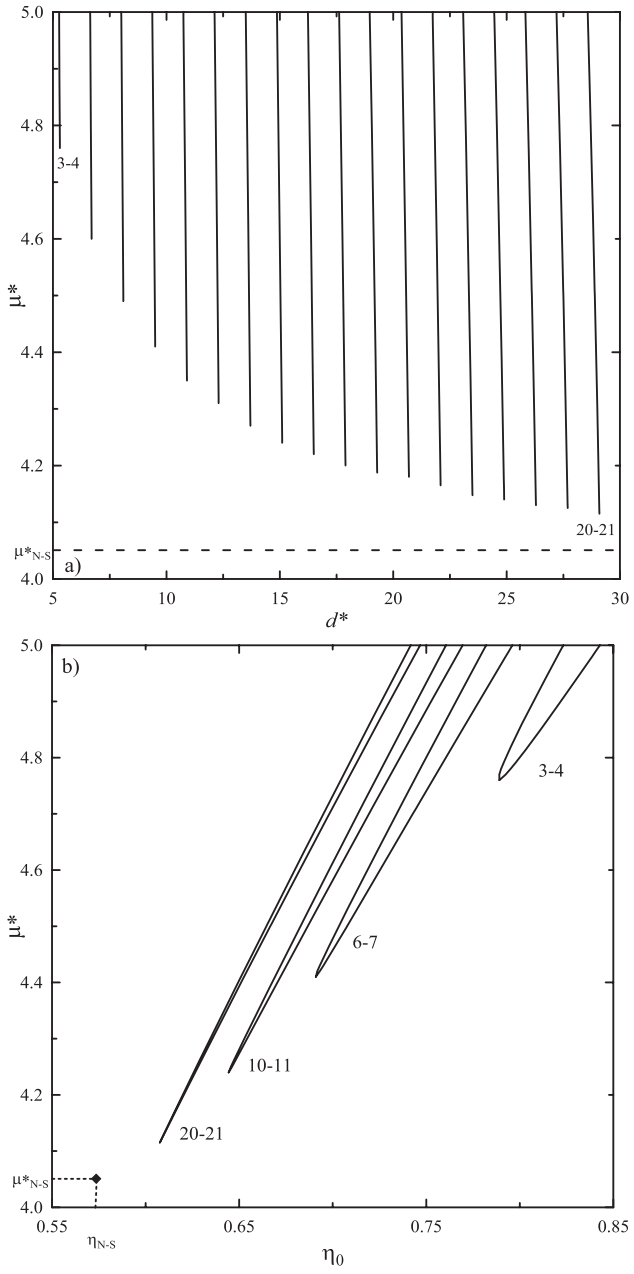

Figure 7. Phase diagram of the system of hard cylinders confined by two hard planar walls. The curves show the phase coexistence between S_i and S_{i+1} smectic-like structures in chemical potential-wall-to-wall separation (a) and chemical potential mean density (b) planes. The values of i range from 3 up to 20. Each layering transition curve is bounded by a lower critical point. With increasing i the chemical potential and the mean density of the critical point moves smoothly down to the bulk values of chemical potential and density ($\mu^*_{\mathrm{N-S}}$ and $\eta_{\mathrm{N-S}}$ shown as dashed lines) of the nematic–smectic A phase transition.

rotating rods also show layering transition and have lower critical points [12]. However, the orientational freedom has a strong effect on the isotropic–nematic and nematic–smectic A capillary phase transitions [13]. The influence of the shape anisotropy on confined systems and the link between layering transition and capillary phase transitions are studied in depth in [13]. Now we turn to the issue of confinement on the second order N–S phase transition.

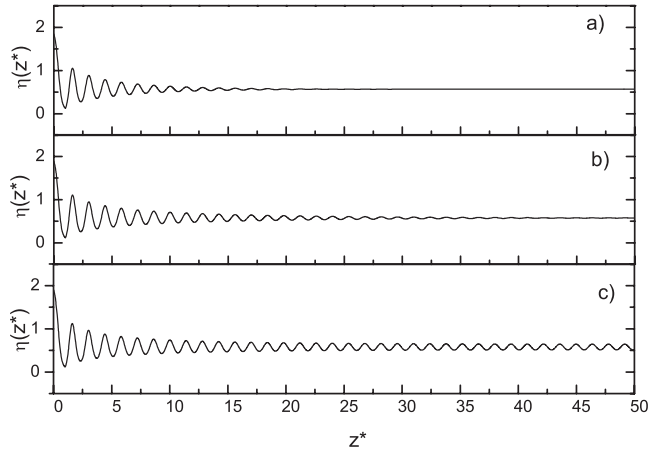

Figure 8. Density profiles of the system of hard cylinders in contact with a hard plane wall at three different chemical potentials: (a) $\mu^* = 3.96$, (b) $\mu^* = 4.0384$ and (c) $\mu^* = 4.0507$.

To understand the behaviour of a fluid confined between two hard walls it is essential to gain some insight into the wetting properties of the fluid in the presence of a single wall. We present our numerically obtained density profiles of parallel cylinders in a semi-infinite system, where the particles are subjected to the following single wall external field:

$$\phi(z) = \begin{cases} \infty, & z < 0 \\ 0, & z \geqslant 0. \end{cases} \tag{16}$$

Note that the Fourier method cannot be applied in this case because the system is non-periodic. On the contrary there is no problem in using the iteration method; one only needs to be careful in specifying the system size, d, which should be large enough not to produce any relevant finite size effects. In our computations $d/L = 1000$ has been used. Figure 8(a) shows the density profile for $\mu^* = 3.96$, the value of which is somewhat smaller than the bulk nematic–smectic chemical potential as obtained from the Onsager theory. We observe a highly oscillating structure close to the wall, associated with the creation of the smectic-like layers, the amplitudes of which are however rapidly damped and beyond a distance about 20 molecular units the density profile is almost constant, i.e. a perfect nematic phase is achieved. By approaching the nematic–smectic coexistence value of the chemical potential, the smectic layers propagate further from the wall, see figure 8(b), and for $\mu^* = \mu^*_{\mathrm{N-S}}$ (figure 8(c)) the wall is completely wet by smectic-like modulation. In order to analyse this behaviour in more detail, we define the following order parameter:

$$S = \max_g S'(g), \tag{17}$$

with

$$S'(g) = \frac{1}{g}\int_0^d \mathrm{d}z\, \rho(z) \cos\left(\frac{2\pi}{g} z\right), \tag{18}$$

where g is a characteristic length. It is known that the above function reflects the oscillatory character of a given density profile, see [15], where a similar order parameter was used, for more details. As an example, we plot $S'(g)$

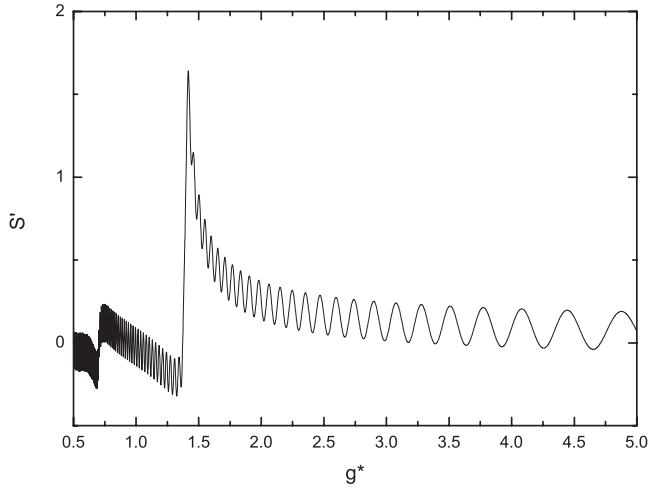

Figure 9. Hard cylinders in contact with a single wall for $\mu^* = 4$. The S' parameter is plotted as a function of g^*. The pair of S' and g^* values at which S' has a maximum corresponds to the order parameter and the mean layer spacing (smectic period), respectively.

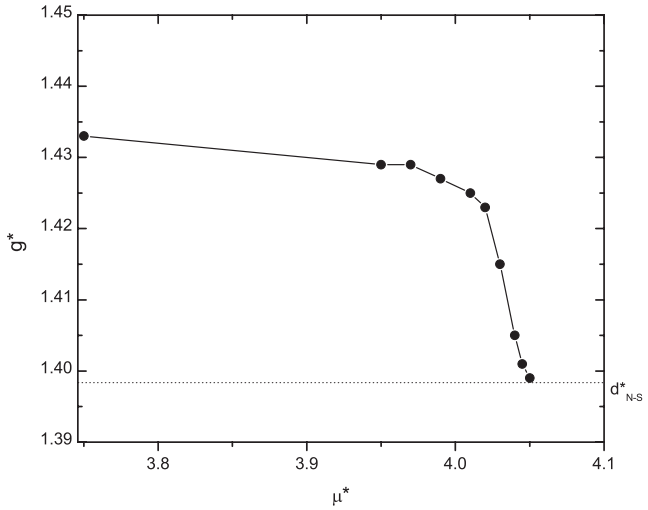

Figure 10. Hard cylinders in contact with a single wall: mean layer spacing as a function of the chemical potential. The solid curve is added as a guide to the eye. The dotted horizontal line indicates the smectic period at the bulk nematic–smectic A phase transition.

as a function of g for $\mu^* = 4$, (see figure 9). The function exhibits a sharp maximum at $g/L = 1.46$. This value is slightly higher than the bulk smectic period. The location of the maximum is an interesting by-product of this analysis and corresponds to the mean layer spacing between two neighbouring layers. Figure 10 shows the chemical potential dependence of g for the interval close to the bulk N–S equilibrium. As expected, the mean period decreases with an increase of the chemical potential and approaches the bulk N–S limit, i.e. $g(\mu \to \mu_{N-S}) = d_{\mathrm{N-S}}$. In order to get more insight into structure of the fluid next to wall, we explore the chemical potential dependence of the order parameter obtained from equations (17) and (18), see figure 11. We observe a continuous increase of S with an increase of the chemical potential; for $\mu^* \to \mu^{*-}_{\mathrm{N-S}}$ the order parameter diverges, which corresponds to the formation of the smectic phase throughout all the system. The inset of figure 11 clearly shows that S diverges logarithmically as $\mu^* \to \mu^{*-}_{\mathrm{N-S}}$. A fit is made by $S = A + B\log(\mu^*_{\mathrm{N-S}} - \mu^*)$, where the values of the parameters are $A = 0.7453$ and $B = -0.711$. These results indicate that the bulk N–S phase transition transforms into a wall induced critical wetting transition.

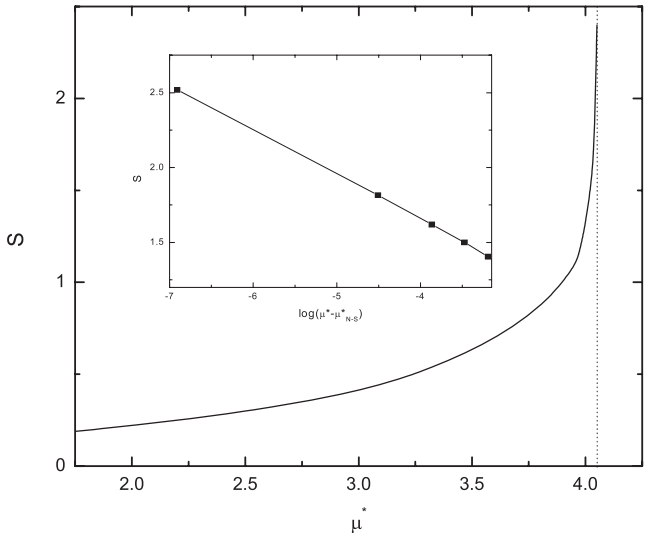

Figure 11. Chemical potential dependence of the order parameter (S) in the presence of a single wall. The inset shows a logarithmic divergence of the order parameter with increasing chemical potential ($\mu^* \to \mu^{*-}_{\mathrm{N-S}}$). At $\mu^{*-}_{\mathrm{N-S}}$ the wall is completely wet by the smectic structure. The dotted vertical line indicates the position of the bulk nematic–smectic A phase transition.

Lastly, we address the issue of the N–S phase transition of the hard parallel cylinders confined by two hard walls. As, according to our calculations above, the corresponding phase transition in the bulk phase is of the second order, the relevant quantity to be analysed is the second derivative of the grand potential presented in the appendix. Figure 12 displays the second derivative of the grand potential for four different sizes of the pore. In figure 12(a) we consider the case of a single wall, i.e. the infinitely large pore. We observe a clear discontinuity at $\mu^*_{\mathrm{N-S}}$ corresponding to the critical wetting by smectic transition (compare with figure 2(b)). For the remaining pores we observe a still rather harsh but continuous change from the nematic regime with just several layers to the regime where the whole pore is filled by the layered structure. One can still speculate about the small discontinuity in the case of $d^* = 500$, but taking into account the dimension of such a pore one can conclude that the presence of the second wall destroys the second order N–S transition. As a result we can say that only the layering transition exists in the slit-like pore. To see other effects, such as the capillary nematization and smectization, the inclusion of orientational freedom is essential.

4. Summary and conclusion

In this work we have studied the influence of confinement on the structure and phase behaviour of an anisotropic hard body

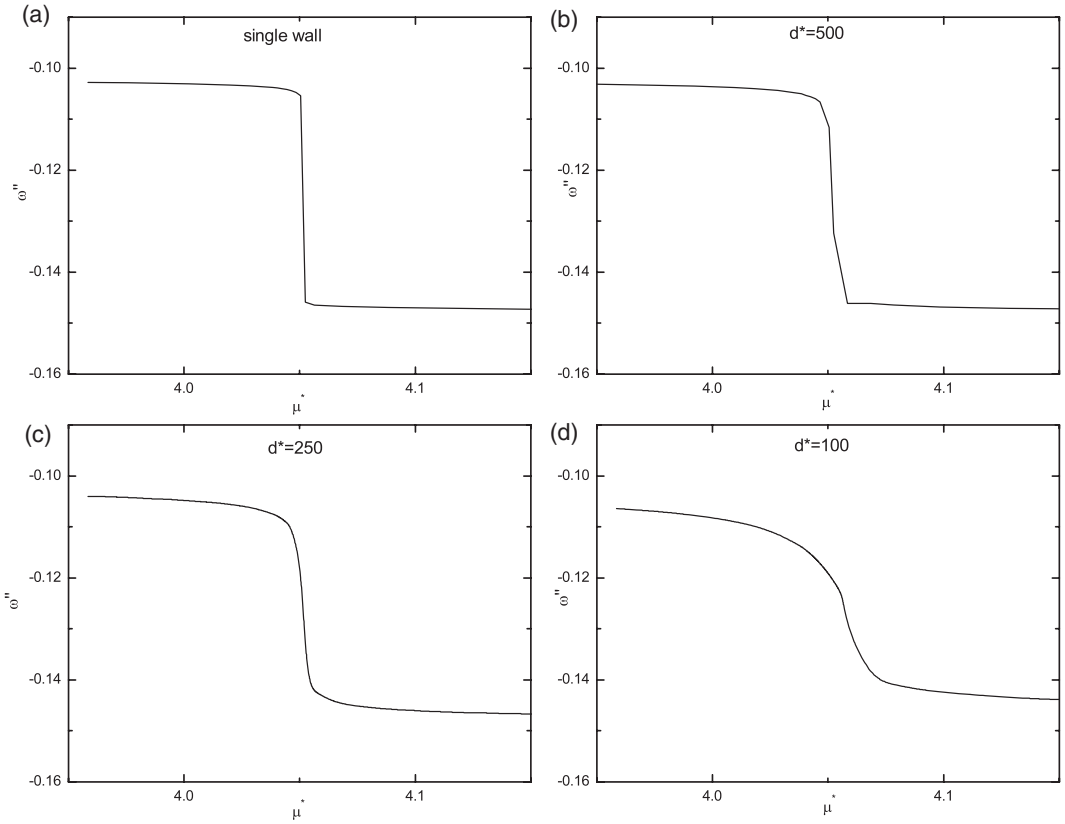

Figure 12. Hard cylinders between two confining hard walls. The second derivative of the grand potential as a function of chemical potential is shown at different wall-to-wall separations. For the definition of ω'' see the caption of figure 2.

fluid. We have adopted perhaps the simplest model, which is the fluid of parallel hard cylinders confined between two parallel hard walls with the assumption of perfect homeotropic anchoring. Formulating Onsager's second virial theory in a form applicable for both bulk and confined systems, we obtained the following results.

- In the case of a single hard wall the system possesses only one free parameter, which is the chemical potential. The presence of a single wall induces a layered structure adjacent to the wall due to the packing effect. For the chemical potential well below its bulk N–S critical value $\mu_{\mathrm{N-S}}$, the smectic phase is unstable; there is only a microscopic smectic-like film adjacent to the wall, the width of which continuously grows with increasing μ. For $\mu \to \mu_{\mathrm{N-S}}$ the thickness of the smectic-like layer logarithmically diverges and the system exhibits a critical wetting transition. By the term 'wetting' we mean a filling of the whole system by the smectic phase. As the wetting transition is of the second order, no prewetting transition (the coexistence between thin and thick smectic films) appears.
- If the fluid is confined between two parallel hard walls, the scenario changes. Now the width of the pore is an additional parameter to the chemical potential. The presence of the second wall suppresses the second order N–S transition and first order layering transitions are produced. The corresponding phase diagram involves a semi-infinite sequence of transition lines corresponding to the coexistence between two structures of completed i and $i + 1$ layers. The layering transition curves are accompanied by lower critical points. Interestingly the critical chemical potential converges to $\mu_{\mathrm{N-S}}$ in the limit $d \to \infty$. The commensuration effect between the layer spacing of the bulk smectic structure and the pore width gives rise to the first order layering transition.
- Our results show that the term 'smectic phase' of confined systems is not obvious. In the bulk, the smectic phase is uniquely defined exhibiting a spatially oscillating density distribution with given amplitude and period, whereas the nematic state does not possess such a structure, i.e. it is spatially homogeneous. Therefore the N–S phase transition can be easily quantified by the Fourier coefficients of the density profiles. On the other hand, confined fluids are always spatially inhomogeneous due to the influence of the external field, which does not allow us to distinguish the smectic and nematic phases. For a fixed pore width, we observe a continuous development from a 'less wavy' structure to a more ordered one with increasing chemical potential. However, no abrupt change is seen even in the second derivative of the grand potential with respect to the chemical potential, which excludes the possibility of first and second order phase transitions. If we associate the reciprocal value of the pore width with the temperature, the situation is analogous to the transition from a low density gas-like state to a high density liquid-like state by following a supersaturated path. We observe that the critical value of the reciprocal pore width is zero.

It is worth noting that our model system in contact with one or two walls resembles the phase behaviour of confined simple fluids. There are close relations between the terms smectic–liquid, nematic–gas, wetting–smectization etc expressions, because the order parameter defined by equations (17) and (18) plays the role of the adsorption. There is, however, one important difference. Whereas the presence of a hard wall leads to a drying (formation of a less ordered phase) in the case of simple fluids, the hard wall induces a smectic-like, i.e. more ordered, phase in our hard cylinder model. The difference stems from the fact that the phase behaviour of our model system is purely entropy driven.

The main output of our study is that even the very simple system of parallel rods can be applied to examine the complex phase behaviour of an anisotropic fluid in the presence of an external field. We believe that the understanding of phase behaviour of this model is a step forward to shedding some light on the essential physics of confined anisotropic fluids. The next steps consist of an investigation of the role of the orientational entropy, the presence of a solvent, attraction forces etc. These problems will be the subject of our future studies.

Acknowledgments

AM would like to acknowledge the financial support of the Ministry of Education, Youth and Sports of the Czech Republic under Project No. LC512 (Center for Biomolecules and Complex Molecular Systems) and the Grant Agency of the Academy of Sciences of the Czech Republic (Grant No. IAA400720710). SV is grateful to Enrique Velasco for useful comments during the course of this study.

Appendix. Determination of the first and second derivative of the grand potential

In order to determine the order of the phase transition in the grand canonical ensemble, we need to examine the behaviour of the first and second derivatives of the grand potential with respect to the chemical potential. Due to the chemical potential dependence of the local density, the first derivative consists of two terms

$$\omega' = \frac{1}{d}\int_0^d \frac{\delta\omega}{\delta\rho(z)}\frac{\partial\rho(z)}{\partial\mu}\mathrm{d}z + \frac{\partial\omega}{\partial\mu}. \tag{A.1}$$

In equilibrium the first term of (A.1) vanishes as a consequence of the Euler–Lagrange equation ($\frac{\delta\omega}{\delta\rho(z)} = 0$). The second term is just the direct derivative of equation (8) with respect to the chemical potential. Therefore, the first derivative of the grand potential density is proportional to the mean density of the system

$$\omega' = -\frac{\beta}{d}\int_0^d \mathrm{d}z\,\rho(z) = -\beta\rho_0. \tag{A.2}$$

In the case of the first order phase transition ω' is discontinuous, while the second order phase transition would only give rise to a kink in ω'. To see more clearly the order of the phase transition, it is customary to determine the second derivative of the grand potential. One can see from equation (A.2) that only the derivative of the local density with respect to chemical potential is required to get ω''. From equation (9) one can prove easily that

$$\frac{\partial\rho(z)}{\partial\mu} = \rho(z)\left(1 - D^2\pi\int_{z-a(z)}^{z+b(z)}\mathrm{d}z'\,\frac{\partial\rho(z')}{\partial\mu}\right), \tag{A.3}$$

and the derivative of equation (A.2) is

$$\omega'' = -\frac{\beta}{d}\int_0^d \mathrm{d}z\,\frac{\partial\rho(z)}{\partial\mu}. \tag{A.4}$$

Equation (A.3) is a self-consistent equation for $\frac{\partial\rho(z)}{\partial\mu}$ and can be solved by iteration once the equilibrium density profile is determined. The advantage of the iterative solution for ω'' is that equations (10), (A.3) and (A.4) enable us to calculate the second derivative of the grand potential at any chemical potential, which is very crucial for the precise location of the phase transition. In addition, there is no need to use finite difference methods for the approximate determination of the first and second derivatives. We use equation (A.4) for the location of the second order phase transition. The discontinuity of ω'' determines the chemical potential where the second order transition takes place.

References

[1] Onsager L 1949 *Ann. New York Acad. Sci.* **51** 627
[2] Vroege G J and Lekkerkerker H N W 1992 *Rep. Prog. Phys.* **55** 1241
[3] McGrother S C, Williamson D C and Jackson G 1996 *J. Chem. Phys.* **104** 6755
[4] Bolhuis P and Frenkel D 1997 *J. Chem. Phys.* **106** 666
[5] Sheng P 1976 *Phys. Rev. Lett.* **37** 1059
[6] van Roij R, Dijkstra M and Evans R 2000 *Europhys. Lett.* **49** 350
[7] Dijkstra M, van Roij R and Evans R 2001 *Phys. Rev.* E **63** 051703
[8] Chrzanowska A, Teixeira P I C, Ehrentraut H and Cleaver D J 2001 *J. Phys.: Condens. Matter* **13** 4715
[9] Reich H and Schmidt M 2007 *J. Phys.: Condens. Matter* **19** 326103
[10] Pineiro M M, Galindo A and Parry A O 2007 *Soft Matter* **3** 768
[11] de las Heras D, Mederos L and Velasco E 2009 *Phys. Rev.* E **79** 011712
[12] de las Heras D, Velasco E and Mederos L 2005 *Phys. Rev. Lett.* **94** 017801
[13] de las Heras D, Velasco E and Mederos L 2006 *Phys. Rev.* E **74** 011709
[14] de las Heras D, Martínez-Ratón Y and Velasco E 2010 *Phys. Rev.* E at press
[15] Steuer H, Hess S and Schoen M 2004 *Phys. Rev.* E **69** 031708
[16] Hosino M, Nakano H and Kimura H 1979 *J. Phys. Soc. Japan* **46** 1709
[17] Mulder B 1987 *Phys. Rev.* A **35** 3095
[18] Veerman J A C and Frenkel D 1991 *Phys. Rev.* A **43** 4334
[19] Capitán J A, Martínez-Ratón Y and Cuesta J A 2008 *J. Chem. Phys.* **128** 194901
[20] Sear R P and Jackson G 1995 *J. Chem. Phys.* **102** 2622
[21] Varga S, Gábor A, Velasco E, Mederos L and Vesely F J 2008 *Mol. Phys.* **106** 1939
Varga S, Velasco E, Mederos L and Vesely F J 2009 *Mol. Phys.* **107** 2481
[22] Ishihara S 2005 *J. Display Technol.* **1** 30